NJC

Accepted Manuscript

ROYAL SOCIETY OF CHEMISTRY

www.rsc.org/njc

Journal Name

ARTICLE

New efficient fused-ring spiro[benzoanthracene-fluorene] dopant materials for blue fluorescent organic light-emitting diodes

Jae-Ryung Cha,[a] Chil-Won Lee[b] and Myoung-Seon Gong[a],*

New blue fluorescent spirobenzoanthracene-type dopant materials, 3,9-di(di(*p*-tolyl))aminospiro[benzo[*de*]anthracene-7,9'-fluorene] (**DTSBAF**) and 3,9-di(di(4-biphenyl))aminospiro[benzo[*de*]anthracene-7,9'-fluorene] (**DBSBAF**) were designed and successfully prepared by an amination reaction of 3-bromo-9-chlorospiro[benzo[*de*]anthracene-7,9'-fluorene] with di(*p*-tolyl)amine and di(4-biphenyl)amine, respectively. The EL characteristics of 1,10-dinaphthylspiro[benzo[*ij*]tetraphene-7,9'-fluorene] (**DNSBTF**) as the blue host material doped with the above blue dopant materials was evaluated. The electroluminescence spectra of indium tin oxide (150 nm)/*N,N'*-diphenyl-*N,N'*-bis[4-(phenyl-m-tolyl-amino)phenyl]-biphenyl-4,4'-diamine (DNTPD, 60 nm)/*N,N,N',N'*-tetra(1-biphenyl)-biphenyl-4,4'-diamine (TBB, 30 nm)/**SBTF** hosts: **SBAF** dopant (20 nm, 5%)/9,10-di(naphthalene-2-yl)anthracen-2-yl-(4,1-phenylene)(1-phenyl-1H-benzo[*d*]imidazole) (LG201, 20 nm)/LiF (1 nm)/Al (200 nm) with **DNSBTF** as a host material show a blue emission band with a full width at half maximum of 50 nm and a λ_{max} = 472 nm. The device obtained from DNSBTF doped with DTSBAF showed a good color purity (0.141, 0.254), high luminance efficiency (10.12 cdA^{-1} at 5 V) and high external quantum efficiency (6.02%).

1. Introduction

Many organic blue light-emitting materials have been studied in order to achieve stability, efficiency, and color purity[1-3]. In particular, a blue emitting material with a high efficiency needs to be developed to reduce the power consumption of organic light-emitting diode (OLED) devices and to increase their color range[4]. A dopant/host emitter system is a common configuration for OLEDs based on small molecules. The energy transfer and charge trapping from the host to the dopant molecule allow the emission to originate from the dopant, and thus, the emission properties are dominated by the dopant. Moreover, the dopant/host system enhances the EL efficiency and the stability of the OLEDs[5-8]. Some blue light-emitting dopants that have been developed include 4,4-bis[2-(4-(*N,N*-diphenylamino)phenyl) vinyl]biphenyl (BDAVBi)[9], p-bis(p-N,N-diphenylaminostyryl)benzene (DSA-Ph)[10], an asymmetrical mono(styryl)amine-based blue dopant (BD-1)[11], diimidazolylstilbenes[12], 2-(styryl)triphenylene derivatives[13], and benzene-cored phenylanthracene derivatives[14]. As a result of the intrinsically wide band-gap, it is not easy to develop new blue-emitting materials with excellent electroluminescence properties. Recently, a diphenylamino fluorene-based blue dopant in a MADN host achieved a very high current efficiency of 11.5 cdA^{-1} with a blue color of CIE$_{x,y}$ (0.17, 0.28)[15,16]. A device doped with iminodibenzyl-distyrylarylene (IDB-Ph) was

reported to achieve a luminance efficiency of 11.0 cdA^{-1} with a color of CIE$_{x,y}$ (0.29, 0.36) and improved thermal stability[17].

Amorphous triarylamines with a high glassy state stability are suitable as host and dopant materials for organic light-emitting devices (OLED). The primary structural feature of an amorphous triarylamine that exhibits high morphological stability is a stable non-coplanar conformation that can effectively inhibit crystallization. However, a chromophore without a rigid planar skeleton usually emits fluorescence with a low quantum yield[18]. Spiro molecules have received a great deal of attention because they have been shown to form thin films of good quality with morphological stability, high glass transition temperatures and amorphous properties[19-24]. In order to produce efficient OLED devices, it is important to improve the quantum yield of the photoluminescence and also to retain the morphological stability of the triarylamine that is used both as a hole transporter and as a dopant.

Spiro[benzo[*c*]fluorene-7,9'-fluorene] (**SBFF**) has an asymmetrical spiro core structure and can be substituted with a variety of substituents. Therefore, its color characteristics can be adjusted by controlling the conjugation length as a host or as a dopant, as shown in Scheme 1[25-28]. Recently, spiro molecules with more fused π-conjugated, spiro[benzo[*ij*]anthracene-7,9'-fluorene] (**SBAF**) have been extensively studied as fluorescent host and dopant materials due to the appropriate chemical modification[29-32].
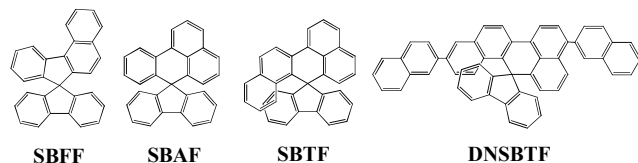
Scheme 1. Fused-ring spiro molecules: **SBFF**, spiro[benzo[*c*]fluorene-7,9′-fluorene]; **SBAF**, spiro[benzo[*de*]anthracene-7,9′-fluorene]; **SBTF**, spiro[benzo[*ij*]tetraphene-7,9′-fluorene] and chemical structure of 1,10-dinaphthyl-**SBTF**

In this study, a novel **SBAF** core structure was developed for use as a highly fluorescent blue dopant material. This material exhibited good thermal/morphological stability, and its optical properties were investigated. In addition, a new highly fused ring spiro[benzo[*ij*]tetraphene-7,9'-fluorene] (**SBTF**) molecule with various aromatic wings, 1,10-dinaphthyl-**SBTF** (**DNSBTF**) was adopted as the blue host material. The electroluminescent properties were evaluated for the multilayered sky-blue OLEDs that were fabricated using the SBTF host material with 3,9-di(di(p-tolyl))amino-**SBAF** (**DTSBAF**) and 3,9-di(di(4-biphenyl))amino-**SBAF** (**DBSBAF**) as the dopant.

2. Experimental

2. 1. Materials and Measurements

Palladium acetate, 9-fluorenone, bromine, sodium *t*-buthoxide, di(4-biphenyl)amine and di(*p*-tolyl)amine (Aldrich Chem. Co., St. Louis, MO, USA) were used as received. 1-Bromo-8-(4-chlorophenyl)naphthalene was prepared by reacting 1,8-dibromonaphthalene with 4-chlorophenylboronic acid via Suzuki coupling. 1,10-Dinaphthylspiro[benzo[*ij*]tetraphene-7,9'-fluorene] (**DNSBTF**) was prepared by using previously reported methods[33-35]. 9,10-*p*-Bis(*p-N,N*-diphenylaminostyryl)benzene (**DSA-Ph**) was used as the dopant material. *N,N'*-diphenyl-*N,N'*-bis[4-(phenyl-*m*-tolyl-amino)phenyl]-biphenyl-4,4'-diamine (DNTPD), *N,N,N',N'*-tetra(1-biphenyl)-biphenyl-4,4'-diamine (TBB), and 9,10-di(naphthalene-2-yl)anthracen-2-yl-(4,1-phenylene)(1-phenyl-1H-benzo[*d*]imidazole) (LG201) were used as a hole injection layer (HIL), hole transfer layer (HTL), and electron transfer layer (ETL), respectively. *n*-Butyllithium (2.5 M solution in *n*-hexane), carbon tetrachloride, potassium carbonate, sodium hydroxide and HCl (Duksan Chem. Co., Seoul, South Korea) were used without further purification. Tetrahydrofuran (THF) and toluene were purified by distillation over sodium metal and calcium hydride. The photoluminescence (PL) spectra were recorded on a fluorescence spectrophotometer (Jasco FP-6500; Tokyo, Japan), and UV-vis spectra were obtained by using a UV-vis spectrophotometer (Shimadzu, UV-1601PC; Tokyo, Japan). The energy levels were measured with a low-energy photo-electron spectrometer (AC-2; Riken-Keiki, Union City, CA, USA), and the FT-IR spectra were obtained with a Thermo Fisher Nicolet 850 spectrophotometer (Waltham, MA, USA). Elemental analyses were performed using a CE Instrument EA1110 (Hindley Green, Wigan, UK), and differential scanning calorimeter (DSC) measurements were performed on a Shimadzu DSC-60 DSC under nitrogen. The thermogravimetric analysis (TGA) was performed on a Shimadzu TGA-50 thermo gravimetric analyzer, and high-resolution mass spectra were recorded using an HP 6890 (Brea, CA, USA) and Agilent Technologies 5975C MSD in a FAB mode (Palo Alto, CA, USA).

2. 2. Preparation of 9-chlorospiro[benzo[de]anthracene-7,9'-fluorene] (CSBAF)

A solution of 1-bromo-8-(4-chlorophenyl)naphthalene (9.72 g, 30.6 mmol) in THF (50 mL) was added to a 250 mL two-necked flask. The reaction flask was cooled to -78 °C, and *n*-BuLi (2.5 M in hexane, 14.68 mL) was added slowly in a dropwise fashion. The solution was stirred at this temperature for 1 h, followed by the addition of a 9-fluorenone solution (5.51 g, 30.6 mmol) in THF (30 mL) under an argon atmosphere. The resulting mixture was gradually warmed to ambient temperature and was quenched by adding saturated aqueous NaHCO$_3$ (90 mL). The mixture was extracted with dichloromethane. The combined organic layers were dried over magnesium sulfate, filtered, and evaporated under a reduced pressure. A yellow powdery product was obtained, and a crude residue was placed in another two-necked flask (100 mL) and dissolved in acetic acid (50 mL). A catalytic amount of aqueous HCl (5 mol%, 12 N) was then added, and the entire solution was heated under reflux for 12 h. After cooling to ambient temperature, the compound was purified as a white powder by silica gel chromatography using dichloromethane/*n*-hexane (2/1).

CSBAF: Yield 78%. FT-IR (KBr, cm^{-1}) 3055, 3032 (aromatic C-H). ^{1}H-NMR (500 MHz, CDCl$_3$) δ 8.21-8.20 (d, 1H), 8.14-8.12 (d, 1H), 7.86-7.83(m, 3H), 7.87-7.67(d, 1H), 7.64-7.61(t, 1H), 7.39-7.36 (t, 2H), 7.24-7-23 (s, 1H), 7.20-7.18 (t, 1H), 7.18-7.13 (t, 2H), 6.97-6.95 (d, 2H), 6.60-6.58 (d, 1H), 6.48-6.47 (d, 1H). Anal. Calcd for C$_{29}$H$_{17}$Cl (Mw, 400.10): C, 86.88; H, 4.27; Cl, 8.84. Found: C, 86.86; H, 4.24; Cl, 8.83. MS (FAB) *m/z* 401.10 [(M + 1)$^+$].

2.3. Preparation of 3-bromo-9-chlorospiro[benzo[de]anthracene-7,9'-fluorene] (BCSBAF)

CSBAF (3.88 g, 10 mmol) was dissolved in carbon tetrachloride in a two-necked flask. Bromine (2.36 g, 15 mmol) was then added slowly in a dropwise fashion over a period of 20 min, and the mixture was then stirred at room temperature for 3 days. The precipitated solid was filtered and dried *in vacuo* to give a crude product that was then purified via recrystallization from ethyl acetate/*n*-hexane (1/1), finally resulting in a white powder.

Yield 86%. FT-IR (KBr, cm^{-1}) 3050, 3035 (aromatic C-H), 748(aromatic C-Br). ^{1}H-NMR (500MHz, CDCl$_3$) δ 8.12-8.08 (t, 2H), 8.06-8.04 (d, 1H), 7.94-9.92 (d, 1H), 7.85-7.84 (d, 2H), 7.40-7.37 (t, 2H), 7.32-7.29 (t, 1H), 7.26-7.24 (d, 1H), 7.16-7.13 (t, 2H), 6.94-6.92 (d, 2H), 6.67-6.65 (d, 1H) , 6.48-6.47 (s, 1H). Anal. Calcd for C$_{29}$H$_{16}$BrCl (Mw, 479.79): C, 72.60; H, 3.36; Br, 16.65; Cl, 7.39. Found: C, 72.57; H, 3.34; Br, 16.62; Cl, 7.38. MS (FAB) *m/z* 481.01 [(M + 1)$^+$].

2.4. Synthesis of 3,9-di(di(*p*-tolyl))amino(spiro[benzo[de]anthracene-7,9'-fluorene] (DTSBAF)

A mixture of **BCSBAF** (6.46 g, 13.47 mmol), di(*p*-tolyl)amine (5.31 g, 26.94 mmol), tri-*tert*-butylphosphine (0.55 g, 2.69 mmol), sodium *tert*-butoxide (3.24 g, 33.68 mmol) and palladium acetate (0.30 g, 1.35 mmol) in toluene (140 mL) was stirred and refluxed under a nitrogen atmosphere for 3 days. Following the removal of the solvent *in vacuo*, an ammonia solution (70 mL) was added, and the mixture was left to stand for 2 h. Dichloromethane (150 mL) and water (100 mL) were added, and the organic phase was separated. The organic solution was washed twice with water (100 mL). The resulting solution was evaporated with a rotary evaporator, and the resulting powdery product was purified via column chromatography by using a mixture of dichloromethane/hexane (v/v, 1/3) as an eluent to produce **DTSBAF** as a yellowish green solid. The other dopant, **DBSBAF**, was prepared using procedures similar to those described above.

DTSBAF: Yield 78%. FT-IR (KBr, cm^{-1}) 3054, 3038 (aromatic C-H), 2930-2850 (alkyl C-H), 1268 (aromatic C-N). ^{1}H-NMR(500MHz, CDCl$_3$) δ 7.99-7.98 (d, 1H), 7.87-7.85 (d, 1H), 7.78-

7.77 (d, 1H), 7.63-7.61 (d, 2H), 7,35-7.33 (d, 1H), 7.26-7.23 (t, 2H) , 7.11-7.08 (t, 2H), 7.02-6.94 (m, 11H), 6.86-6.84 (d, 4H), 6.82-6.80 (d, 1H), 6.73-6.72 (d, 4H), 6.54-6.53 (d, 1H), 6.14 (s, 1H), 2.26 (s, 12H). ^{13}C-NMR(500MHz, CDCl$_3$) δ 156.38 , 147.19, 146.41, 144.29, 142.92, 139.77, 139.45, 137.89, 132.49, 131.47, 130.95, 129.75, 129.67, 128.85 , 128.30, 128.21, 127.30, 127.15, 126.58, 125.35, 125.19, 124.79, 124.52, 124.07, 123.05, 121.99, 120.72, 120.54, 120.06, 118.88, 59.88, 20.88, 20.79. Anal. Calcd for C$_{57}$H$_{44}$N$_2$ (Mw, 756.35): C, 90.44; H, 5.86; N, 3.70. Found: C, 90.37; H, 5.83; N, 3.68. MS (FAB) m/z 767.35 [(M+1)$^+$]. UV-vis (THF): λ_{max} (Absorption)= 418 nm, λ_{max} (Emission)= 472 nm.

DBSBAF: Yield 71%. FT-IR (KBr, cm^{-1}) 3050, 3035 (aromatic C-H), 1265 (aromatic C-N). ^{1}H-NMR(500MHz, CDCl$_3$) δ 8.15-8.13 (d, 1H), 8.05-8.03 (d, 1H), 7.87-7.85 (d, 1H), 7,76-7.72 (m, 6H), 7.58-7.53 (m, 6H), 7.51-7.49 (d, 1H), 7.47-7.45 (d, 1H), 7,42 (s, 1H), 7.39-7.29 (m, 13H), 7.30 (s, 1H), 7.25 (s, 2H), 7.21-7.17 (t, 2H), 7.12-7.08 (t, 4H), 7.01-6.99 (t, 2H), 6.56-6.54 (d, 1H), 6.35 (s, 1H). ^{13}C NMR (CDCl$_3$) δ 156.1, 146.1, 144.3, 142.7, 139.9, 139.6, 137.9, 134.4, 134.1, 130.3, 129.8, 129.1, 129.0, 128.8, 128.6, 128.2, 127.6, 127.5, 127.4, 127.1, 126.0, 125.5, 125.2, 124.7, 124.4, 124.3, 124.2, 123.3, 122.9, 122.2, 122.0, 120.9, 120.1, 119.1, 118.1, 59.8. Anal. Calcd for C$_{69}$H$_{44}$N$_2$ (Mw, 900.35): C, 91.97; H, 4.92; N, 3.11. Found: C, 91.94; H, 5.18; N, 2.76. MS (FAB) m/z 901.35 [(M+1)$^+$]. UV-vis (THF): λ_{max} (Absorption)= 421 nm, λ_{max} (Emission)= 472 nm.

2. 5. OLED fabrication

A basic device configuration with ITO (150 nm)/*N,N'*-diphenyl-*N,N'*-bis[*4*-(phenyl-*m*-tolyl-amino)phenyl]-biphenyl-*4,4'*-diamine (DNTPD, 60 nm)/*N,N,N',N'*-tetra(1-biphenyl)-biphenyl-*4,4'*-diamine (TBB, 30 nm)/**SBTF** host: **DTSBAF** or **DBSBAF** (20 nm, 5%)/LG201 (20 nm)/LiF (1 nm)/Al (200 nm) was used to fabricate the devices, as shown in Fig. 1. The organic layers were sequentially deposited from heated alumina crucibles onto the substrate at a rate of 1.0 Å/s via thermal evaporation. The concentration of the dopant materials varied at 5%, and the devices were encapsulated with a glass lid and a CaO getter after cathode deposition. The current density–voltage luminance and EL characteristics of the blue fluorescent OLEDs were measured with a Keithley 2400 source measurement unit (Cleveland, OH, USA) and a CS 1000 spectroradiometer.
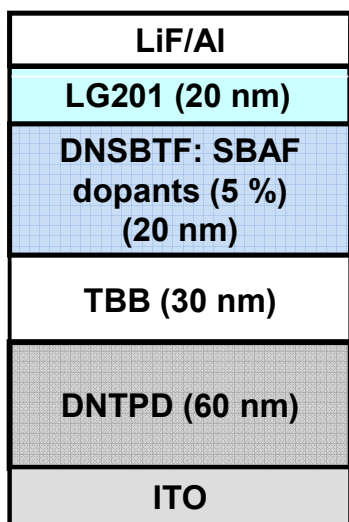

3. Results and discussion

3. 1. Synthesis and characterization

The host material, 1,10-dinaphthylspiro[benzo[*ij*]tetraphene-7,9'-fluorene] (**DNSBTF**), was prepared by using multi-step synthetic routes, as previously reported[33-35]. New dopant materials, 3,9-di(di(*p*-tolyl))aminospiro[benzo[*de*]anthracene-7,9'-fluorene] (**DTSBAF**) and 3,9-di(di(4-biphenyl))aminospiro[benzo[*de*]anthracene-7,9'-fluorene] (**DBSBAF**), were prepared through (1) the Suzuki reaction of 1-bromo-8-(4-chlorophenyl)naphthalene with 4-chlorophenylboronic acid, (2) the coupling reaction of 8-(4-chlorophenyl)-1-lithionaphtalene and 9-fluorenone, (3) the cyclization reaction, and (4) an amination reaction of 3-bromo-9-chlorospiro[benzo[*de*]anthracene-7,9'-fluorene] (**BCSBAF**) with diarylamino compounds. Yields of 78% (**DTSBAF**) and 71% (**DBSBAF**) were achieved in the presence of a palladium acetate catalyst, as shown in Scheme 2. The chemical structures and the compositions of the resulting **SBAF** dopants were characterized via ^{1}H-NMR, ^{13}C-NMR, FT-IR spectroscopy, elemental analysis, and gas chromatography-mass spectrometry (Fig. S1-S10). A chiral carbon peak was observed at about 60.0 ppm in the ^{13}C NMR spectra. The results of the elemental analysis and the mass spectroscopy also indicated that **DTSBAF** and **DBSBAF** had formed, and the observations were consistent with the calculated data.
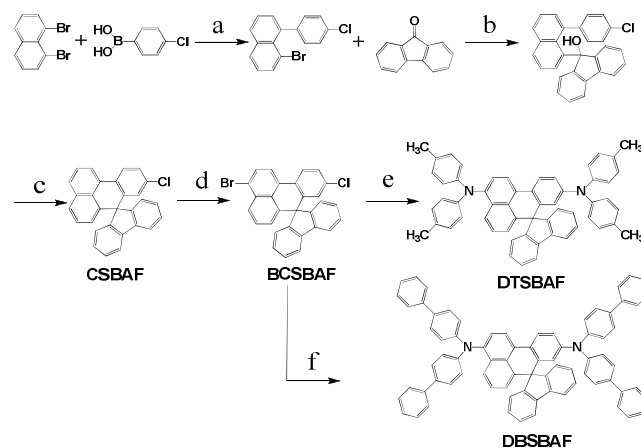
Scheme 2. Preparation of **DTSBAF** and **DBSBAF** dopant materials with **SBAF** core; a: Pd cat, K$_2$CO$_3$, THF/H$_2$O, reflux, 24 h; b: *n*-BuLi, THF, -78°C, 3 h; c: HCl/AcOH, reflux, 6 h; d: Br$_2$, CCl$_4$, 20 ^{o}C, 24 h; e: di(*p*-tolyl)amine, Pd(Ac)$_2$, t-BuONa/toluene,130 ^{o}C, 36 h; f: di(4-biphenyl)amine, Pd(Ac)$_2$, t-BuONa/toluene,130 ^{o}C, 36 h.

3. 2. Optical properties

DTSBAF and **DBSBAF** are light greenish yellow powders and can easily form an amorphous transparent film when spin-coated. Both a THF solution and a solid film of **DTSBAF** and **DBSBAF** emit strong blue photoluminescence (PL) under irradiation with a general UV lamp (365 nm). The UV-vis absorption and PL spectra of the **DTSBAF** and **DBSBAF** dopant materials including the **DNSBTF** host are summarized in Fig. 2 and Table 1. **DTSBAF** and **DBSBAF** solutions had maximum UV absorption peaks at 418 and 421 nm, respectively, and both had blue emission at 472 nm, as shown in Figs. 2a and 2b. In the film state, the maximum absorption

Fig. 1. Basic device configuration for fluorescent sky-blue lighting OELD.

peaks of **DTSBAF** and **DBSBAF** were located at 424 and 426 nm, respectively, and the PL peaks for both were at 475 nm. These show UV–vis peaks at a somewhat longer wavelength, suggesting the presence of certain intermolecular electronic interactions. The degree in the red shift is considerably smaller than that observed with π-conjugated compounds that take face-to face stacking[36]. Di(*p*-tolyl)amine groups were introduced into the 3- and 9-positions in **SBAF** [λ_{max} (absorption) = 312, 327 and 341 nm] core and caused a red-shift in the absorption spectra, even as the electron donating property increased. This implies that the substitution in the **SBAF** core somewhat increased due to the incorporation of the diarylamine groups at both ends of the **SBAF** unit. The fused-ring host material, **DNSBTF** solution had maximum UV absorption peaks at 387 nm and blue emission of about 442 nm, whereas the solid state PL maxima were observed at 449 nm (Fig. 2c).
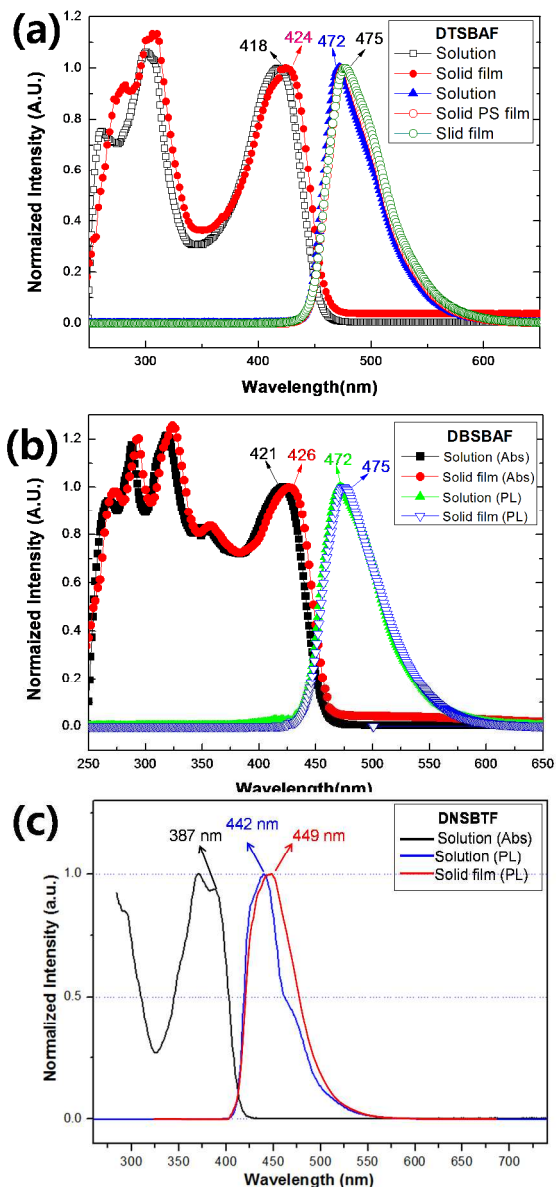

Fig. 2. UV-vis and PL spectra of (a) **DTSBAF**, (b) **DBSBAF**, and **DNSBTF**.

3. 3. Thermal properties.

The operational stability of an OLED is directly related to the thermal stability of the light-emitting layer. Thus, a high glass transition temperature (T_g) indicates that the morphology of the material will not easily change due to the high temperatures generated during operation of the OLED devices[37,38]. Table 1 summarizes the T_g values and the decomposition temperature (T_d) of the diarylamine-substituted **SBAF** derivatives. No melting points were observed during the second heating, even though the purified samples were given enough time to cool in air. Once the sample became an amorphous solid, it did not revert to its crystalline state. After the sample had cooled to room temperature, a second DSC scan at 10 °C/min revealed a T_g at 148 and 186 °C, respectively. In comparison to **DTSBAF**, the incorporation of the biphenyl group on the **SBAF** unit led to higher T_g and T_d values. Nevertheless, the presence of the diarylamine side groups meant that these **SBAF** derivatives exhibited a higher T_g than other well-known blue-dopant materials, 9,10-*p*-bis(*p*-N,N-diphenyl-aminostyryl)benzene (**DSA-Ph**, 89 °C) and iminodibenzyl-phenyldistyrylarylene (**IDB-Ph**, 119 °C)[10,17]. Consequently, these amorphous glassy state films of diarylamine-substituted **SBAF** derivatives were capable of forming morphologically stable and uniform amorphous films that were required to improve the efficiency of OLED devices.

Table 1. UV absorption, PL, energy levels and thermal properties of a host and two dopants.

Properties	Sample		DNSBTF	DTSBAF	DBSBAF
Purity[a]	HPLC	(%)	99.9	99.9	99.9
Thermal Analysis	DSC	T_g (°C)	179	148	186
		T_d (°C)	322 (T_m)[e]	412	449
Optical Analysis	UV (THF)	Max (nm)	387 (391)[f]	418 (424)[f]	421 (426)[f]
		Bg[b] (eV)	3.00	2.70	2.71
	PL (THF)	Max (nm)	442	472	472
		FWHM[c] (nm)	43	56	57
	PL (Solid)	Max (nm)	449	475	475
		FWHM[c] (nm)	53	58	58
Electrical Analysis	AC-2[d]	HOMO (eV)	5.82	5.31	5.42
		LUMO (eV)	2.82	2.61	2.71

[a]The purity of the samples were finally determined by high performance liquid chromatography (HPLC) using the above prepared samples after train sublimation; [b]Bandgap; [c]Full width at half maximum; [d]AC-2 (60 nm film); [e]melting temperature; [f]solid film

3. 4. Energy levels and theoretical calculations

The energy levels of the two dopant materials that were used to fabricate the OLEDs are shown in Fig. 3. A low-energy photoelectron spectrometer was used to obtain information on the HOMO energies of the host and dopant materials and to examine the charge injection barriers (Fig. S11). The energy gaps calculated for **DTSBAF**, **DBSBAF**, and **DNSBTF** were 2.70, 2.71 and 3.00 eV, respectively. The dopant **DTSBAF** with the highly donating group had the lowest band gap of 2.70 eV. The highest occupied molecular orbital (HOMO) energy levels were −5.31, −5.42 and −5.82 eV for **DTSBAF, DBSBAF** and **DNSBTF,** respectively. The HOMO value of **DTSBAF** was lower than those for **DTSBAF** and commercial **DSA-Ph** (−5.42 and −5.40 eV)[10].

Fig. 4 shows the geometric structure of **DTSBAF** and **DBSBAF**. The flanking diarylamine appendages at both the C3 and C9 positions in the **SBAF** backbone are turned (68° and 66°) to avoid a

steric interaction between the nitrogen lone pairs and **SBAF** core for **DTSBAF** and **DBSBAF**. The twisted geometry could efficiently prevent the recrystallization in the film due to the large torsional stresses, which can induce the formation of either an exciplex or excimer[39].

A molecular simulation also showed the electron distribution of two **SBAF** dopant materials. The HOMO and the lowest unoccupied molecular orbital (LUMO) distribution for **DTSBAF** and **DBSBAF** are shown in Fig. 6. The HOMO orbital was distributed throughout the diarylamine and the **SBAF** core, whereas the LUMO orbitals were concentrated in the **SBAF** core. The substitution of fluorene did not affect the HOMO and the LUMO distribution in the dopant materials.
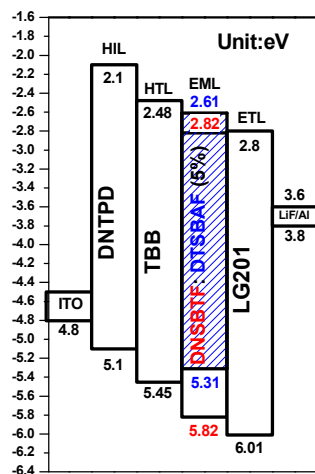

Fig. 3. Energy diagram of the sky-blue fluorescence device using **DNSBTF**: **5% DTSBAF** dopant. (EIL)
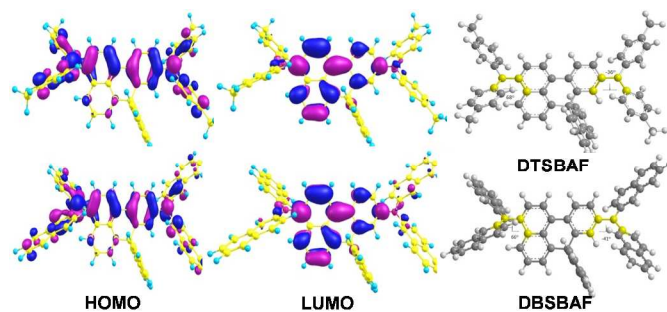

Fig. 4. HOMO and LUMO electronic density distributions of **DTSBAF** and **DBSBAF**, calculated at the DFT/B3LYP/6-31G* for optimization and Time Dependent DFT (TDDFT) using Gaussian 03.

3. 5. EL properties.

The EL spectra of the blue fluorescent **DNSBTF** devices doped with **SBAF** and **DSA-Ph** dopants at concentrations of 5% showed a maximum peak at 472 nm, as shown in Fig. 5 and Table 2. The EL spectra of the two devices doped with **DTSBAF** and **DBSBAF** dopant materials were different from that of **DSA-Ph**, with a shoulder at 490 nm. A sky blue emission was observed, and the color coordinates of the devices based on **DNSBTF: DTSBAF** and **DBSBAF** were (0.141, 0.254) and (0.136, 0.214), respectively (Fig. 6). The EL peaks of the **DTSBAF** and **DBSBAF** devices were consistent with the PL spectra of the two dopants[40-42]. The EL emission was dominated by the emission peak of the dopant, suggesting that the energy transfer from the host to the dopant was quite efficient at the optimum dopant concentration employed in this experiment. A full width at half maximum (FWHM) of 50 nm was relatively constant and led to sky blue, as shown in the PL spectrum (58 nm). In addition, the similarity and shape between the PL and EL spectra of the two **SBAF** dopants indicates that the blue EL was also a result of the emission by **SBAF** dopants, which means that the Förster energy transfer from the host to the dopant is very efficient[38,39].
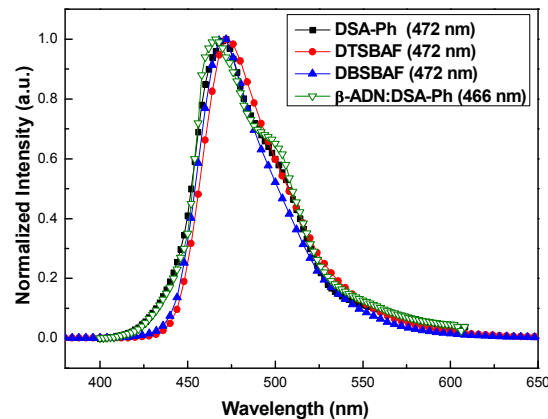

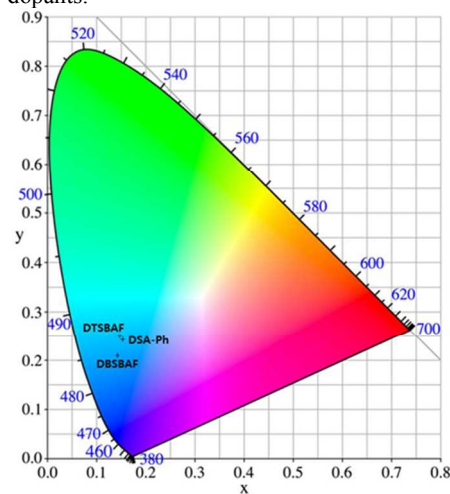**Fig. 5**. Electroluminescence spectra of devices using **DNSBTF** host and **SBAF** dopants.

Fig. 6. CIE coordinates for the devices using **DNSBTF** host and **SBAF** dopants.

3. 6. OLED device properties.

The device properties were examined by fabricating multilayer devices with the **SBTF** host and three dopant materials, including commercial **DSA-Ph**, using the following configuration: glass ITO anode/HIL/HTL/EML/ETL/LiF/Al cathode. **DNTPD** was used as the HIL, **TBB** as the HTL, **DNSBTF** host: 5% dopant as the EML and **LG201** as the ETL, and a 10 Å LiF layer was used as the EIL. Fig. 7 shows the luminance–voltage–current density characteristics of the OLEDs with **DNSBTF** and 5% **SBAF** dopants. Although the dopant **DTSBAF** had a band gap of 2.70 eV, it showed a slightly lower current density and a higher luminance than that of **DBSBAF** at the same driving voltage. The threshold voltage for the luminescence is of about 3.5 V, at which point the electrons and the holes appear to reach the light-emitting layer. For all devices, no light emission occurs below this voltage. As shown in Fig. 8, the

luminance efficiency curves of the devices obtained from **DTSBAF** and **DBSBAF** show 10.12 and 7.62 cdA^{-1}, respectively. A high efficiency (>10.12 cdA^{-1}) was obtained for the **DTSBAF** device, as shown in Table 2. All devices exhibited a moderate current density before the turn-on voltage due to the absence of a shunt resistance. Although the CIE value of the device using **DNSBTF: DTSBAF** was similar to that of the **DSA-Ph** device, its luminance efficiency was higher than that of the **DSA-Ph** device, which was of 7.27 cdA^{-1} at 5 V.
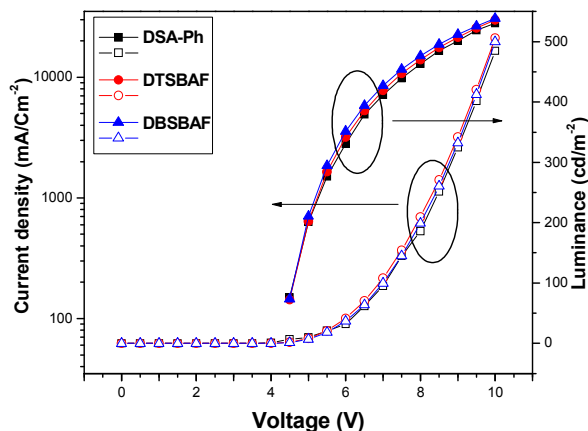

Fig. 7. Current density-voltage-luminance characteristics of the devices using **DNSBTF** host materials doped with 5 % **SBAF** dopants.
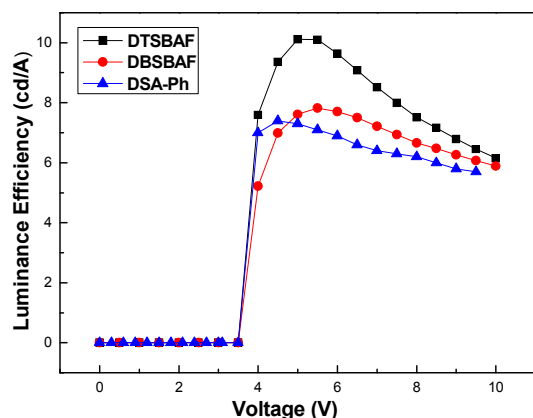

Fig. 8. Luminance efficiency-voltage characteristics of the device using **DNSBTF** host doped with 5% **SBAF** dopants.

Table 2. Eelectroluminescence properties of the devices obtained from three dopant materials.

Materials	Host	DNSBTF		
Properties	Dopant (%)	DSA-Ph	DTSBAF 5%	DBSBAF
EL at 5 V	λ_{max} (nm)	472	472	472
	FWHM (nm)	56	50	51
	mA/cm^{-2}	14.58	6.98	8.36
	cdA^{-1}	7.27	10.12	7.62
	cdm^{-2}	907	706	637
	CIE$_x$	0.151	0.141	0.136
	CIE$_y$	0.245	0.254	0.214
	EQE(%)	4.35	6.02	5.07

The external quantum efficiency (EQE) of the devices obtained from the **DNSBTF** doped with 5% **DTSBAF** and **DBSBAF** was of 6.02 and 5.07%, respectively. We can see from Fig. 9 that the device

using a 5% doping concentration of **DTSBAF** has a higher efficiency than the device with **DBSBAF** (5.07%) and the device with **DSA-Ph** (4.35%). The device based on **DTSBAF** showed a maximum power efficiency of 6.35 lm/W with x=0.141 and y=0.254, and the efficiency increased rapidly to a maximum of approximately 10.12 cdA^{-1} at a low current density of 6.98 mAcm^{-2} at 5 V.

The dependence of the chromatic variation of the device on the current density was measured to evaluate its stability (Fig. 10). The EL spectrum was converted into chromaticity coordinates on the CIE 1931 diagram, and the results indicated an increased stability in the chromaticity with an increase in current density or in the applied voltage. All three of these dopants show differences in terms of the changes in chromaticity with respect to the current density. As with the 5% blue dopant, the change in the chromaticity with the current density also increased. In addition, the stability in the CIE$_x$ coordinates was better than that of CIE$_y$. In particular, the magnitude in the color shift of the **DTSBAF** and **DBSBAF** was smaller than that of the **DSA-Ph**.
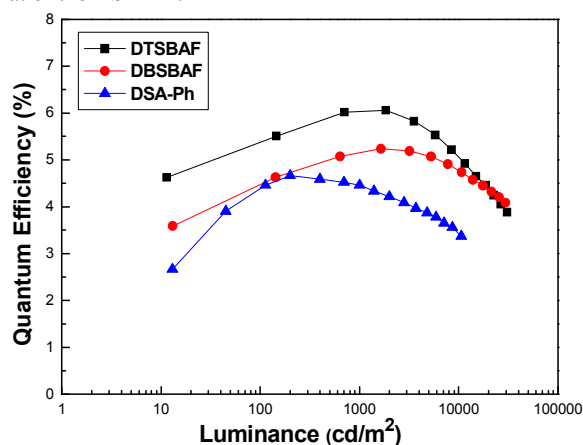

Fig. 9. Quantum efficiency–luminance curves of the **DNSBTF** host doped with 5% **SBAF** dopants.

The holes were injected from the hole transfer layer, **DNTPD**, were transferred to the light emitting layer, and were trapped at the dopant sites. The two blue **SBAF** dopants had a large capacity to catch the holes and minimized the loss of the holes, resulting in good EL efficiency. Thus, the HOMO level for **DTSBAF** or **DBSBAF** as a dopant was suitable for hole trapping and hole transport, and the **SBTF** host had moderate properties for balancing holes and electrons in the emitting layer. These results suggest that an exciton was formed and that light was emitted at specific thresholds.
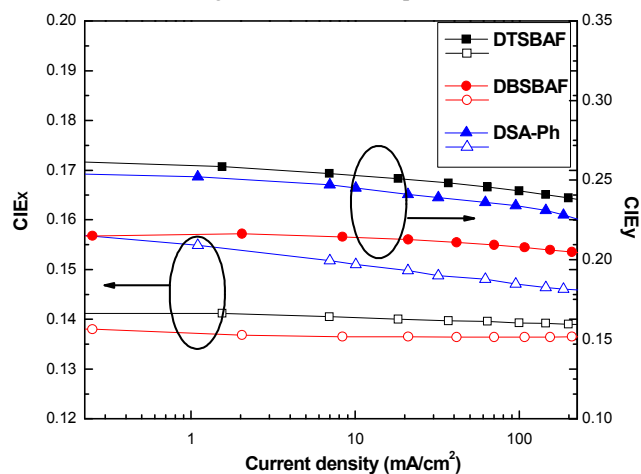

Fig. 10. Stability of the chromaticity depicted by CIE coordination

for the devices using **DNSBTF** host doped with 5% **DTSBAF**, **DBSBAF** and **DSA-Ph** dopants.
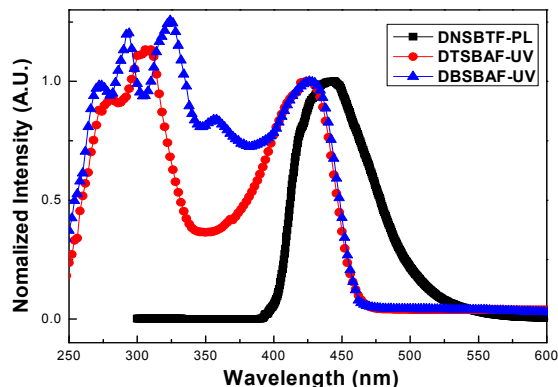

Fig. 11. Overlapped UV-vis absorption spectra of **DTSBAF** and **DBSBAF** dopants and PL spectrum of the **DNSBTF** host.

Fig. 11, the absorption spectra of **DTSBAF** and **DBSBAF** overlaps the greater part of PL spectrum of **DNSBTF**, which indicates that the energy transfer from **DNSBTF** to **DTSBAF** and **DBSBAF** should effectively take place in doped devices[41,42]. A combination of good efficiency and good color purity indicates that the fused ring spiro host and dopant materials are good candidates as sky blue OLED emitters.

The lifetime values of the devices **DTSBAF**, **DBSBAF** and **DSA-Ph** were measured as the operational lifetime ($t^{1/2}$) of the sky-blue devices at a constant current (5 mA/cm^2). Lifetime (150 h) of **DBSBAF** was more than that of **DNSBTF**: 5% **DSA-Ph** (113 h), which can be explained by the more stable morphology of the **DTSBAF** and **BDSBAF** dopant material. Especially **DBSBTF** shows lower stability (133 h) than that of **DBSBAF**.

4. Conclusions

We have successfully designed and synthesized two novel fused ring spiro dopant materials, **DTSBAF** and **DBSBAF**, in which the donor diarylamine groups were substituted into the C3 and C9 position of the **SBAF** backbone. The rigidity of the **SBAF** core could be beneficial for improving the morphological stability and for endowing sufficiently high efficiency for a wide range of fluorescence dopants. The EL emission spectra of the devices were of about 472 nm, and the typical OLED devices showed excellent performance. The **SBAF**-based device exhibited a highly-efficient sky blue light emission with a maximum efficiency of 10.12 cdA^{-1} (EQE, 6.02%) at 5 V. These characteristics indicate that these blue light emitting materials are adequate for use in fluorescent OLED applications.

Notes and references

[a]Department of Nanobiomedical Science and BK21 PLUS NBM Global Research Center, Dankook University, Chungnam 330-714, Republic of Korea.
[b]Department of Polymer Science and Engineering, Dankook University 126, Jukjeon-dong, Suji-gu, Yongin, Gyeonggi 448-701, Republic of Korea.

1   Z.-Q. Gao, B.-X. Mi, C.-H. Chen, K.-W. Cheah, Y.-K. Cheng and W.-S. Wen, *Appl. Phys. Lett.*, 2007, **90**, 123506.

2   M.-T. Lee, H.-H. Chen, C.-H. Lian, C.-H. Tsai and C.-H. Chen, *Appl. Phys. Lett.*, 2007, **85**, 3301.

3   S. Tao, Z. Hong, Z. Peng, W. Ju, X. Zhang, P. Wang, S. Wu and S. Lee, *Chem. Phys. Lett.*, 2004, **397**, 1.

4   S.-W. Wen, M.-T. Lee and C.-H. Chen, *J. Displ. Technol.*, 2005, **1**, 90.

5   C.W Tang, S.A VanSlyke and C.-H. Chen, *J. Appl. Phys.*, 1989, **65**, 3610.

6   J.-M. Shi and C.-W Tang, *Appl. Phys. Lett.*, 1997, **70**, 1665.

7   L.-S. Hung and C.-H. Chen, *Mater. Sci. Eng.*, 2002, **R 39**, 143.

8   J.-M. Shi and C.-W. Tang, *Appl. Phys. Lett.,* 2002, **80**, 3201.

9   C.-L. Li, S.-J. Shieh, S.-C. Lin and R.-S. Liu, *Org. Lett.*, 2003, **5**, 1131.

10   M.-T. Lee, H.-H. Chen, C.-H. Liao, C.-H. Tsai and C.-H. Chen, *Appl. Phys. Lett.*, 2004, **85**, 3301.

11   M.-T. Lee, C.-H. Liao, C.-H. Tsai and C.-H. Chen, *Adv. Mater.*, 2005, **17**, 2493.

12   P.-Y. Chou, H.-H. Chou, Y.-H. Chen, T.-H. Su, C.-Y. Liao, H.-W. Lin, W.-C. Lin, H.-Y. Yen, I.-C. Chen and C.-H. Cheng, *Chem. Commun.*, 2014, **50**, 6869

13   H.-H. Chou , Y.-H. Chen, H.-P. Hsu , W.-H. Chang, Y.-H. Chen, and C.-H. Cheng, *Adv. Mater.*, 2012, **24**, 5867.

14   J.-Y. Hu , Y.-J. Pu, F. Satoh , S. Kawata , H. Katagiri , H. Sasabe, and J. Kido, *Adv. Funct. Mater.*, 2014, **24**, 2064.

15   K.-H. Lee, Y.-S. Kwon, L.-K. Kang, G.-Y. Kim, J.-H. Seo, Y.-K. Kim and S.-S. Yoon, *Synth. Metals* 2009, **159**, 2603.

16   Y.-S. Kwon, K.-H. Lee, G.-Y. Kim, J.-H. Seo, Y.-K. Kim and S.-S. Yoon, *J. Nanosci. Nanotechnol.*, 2009, **9**, 7096.

17   M.-H. Ho, C.-M. Chang, T.-Y. Chu, T.-M. Chen and C.-H. Chen, *Org. Electron.*, 2008, **9**, 101.

18   N.I. Nizhegorodov and W.S. Downey, *J. Phys. Chem.*, 1994, **98**, 5639.

19   J. Salbeck, N. Yu, J. Bauer, F. Weissörtel and H. Bestgen, *Synth Metals* 1997, **91**, 209.

20   D.F. O'Brien, P.E. Burrows, S.R. Forrest, B.E. Konne, D.E. Loy and M.E. Thompson, *Adv. Mater.*, 1998, **10**, 1108.

21   J. Salbeck, J. Bauer and F Weissörtel, *Macromol. Symp.*, 1997, **125**, 121.

22   K. Katsuma and Y. Shirota, *Adv. Mater.*, 1998, **10**, 23.

23   U. Bach, K.D. Cloedt, H. Spreitzer and M. Gratzel, *Adv. Mater.*, 2000, **12**, 1060.

24   C.-W. Ko and Y.-T. Tao, *Synth. Metals* 2002, **126**, 37.

25   K.-S. Kim, Y.-M. Jeon, J.-W. Kim, C.-W. Lee and M.-S. Gong, *Org. Electron.*, 2008, **9**, 797.

26   S.-O. Jeon, Y.-M. Jeon, J.-W. Kim, C.-W. Lee and M.-S. Gong, *Org. Electron.*, 2008, **9**, 522.

27   Y.-M. Jeon, J.-W. Kim, C.-W. Lee and M.-S. Gong, *Dyes Pigments* 2009, 83, 66.

28   K.-S. Kim, H.-S. Lee, Y.-M. Jeon, J.-W. Kim, C.-W. Lee and M.-S. Gong, *Dyes Pigments* 2009, **81**, 174.

29   H. Liang, X. Wang, X. Zhang, Z. Ge, X. Ouyang and S. Wang, *Dyes Pigments* 2014, **108**, 57.

30   J.-Y. Kim, C.-W. Lee, J.-G. Jang and M.S. Gong, *Dyes Pigments* 2012, **94**, 304.

31   M.-J. Kim, C.-W. Lee and M.-S. Gong, *Dyes Pigments*, 2014, **105**, 202.

32   H. Liang, X. Wang, X. Zhang, Z. Liu, Z. Ge, X. Ouyang and S. Wang,

New J. Chem., 2014, **38**, 4696.

33   J.-R. Cha, C.-W. Lee and M.-S. Gong, *J. Fluoresc.*, 2014, **24**. 1215.

34   M.-J. Kim, C.-W. Lee and M.-S. Gong, *Bull. Korean Chem. Soc.*, 2014, **35**, 1639.

35   M.-J. Kim, C.-W. Lee and M.-S. Gong, *Org. Electron.*, 2014, **15**, 2922.

36   M.T. Bernius, M. Inbasekaran, J. O'Brien and W. Wu, *Adv. Mater.*, 2000, 12, 1737.

37   K. Danel, T.-H. Huang, J.-T. Lin, Y.-T. Tao and C.-H. Chuen, *Chem. Mater.*, 2002, **14**, 3860.

38   H. Aziz and Z.D. Popovic, *Chem. Mater.*, 2004, **16**, 4522.

39   I. Cho, S.H. Kim, J.H. Kim, S. Parka, and S.Y. Park, *J. Mater. Chem.*, 2012, **22**, 123.

40   M.-T. Lee, H.-H. Chen, C.-H. Liao, C.-H. Tsai and C.-H. Chen, *Appl. Phys. Lett.*, 2004, **85**, 3301.

41   M.-H. Ho, Y.-S. Wu, S.-W. Wen, M.-T. Lee, T.-M. Chen, C.-H. Chen, K.-C. Kwok, S.-K. So, K.-T. Yeung, Y.-K. Cheng, and Z.-Q. Gao, *Appl. Phys. Lett.*, 2006, **89**, 252903.

42   M.-T. Lee, C.-H. Liao, C.-H. Tsai and C.-H. Chen, *Adv. Mater.*, 2005, **17**, 2493.